VERTAISARVIOITU
KOLLEGIALT GRANSKAD
PEER-REVIEWED
www.tsv.fi/tunnus

Numerical modelling of pore-fluid-enhanced thermal spallation in granitic rock

Timo Saksala

Summary This paper considers numerically the effect of pore-fluid on thermal spallation of granitic rock. For this end, a numerical model based on the embedded discontinuity finite element approach to rock fracture and an explicit scheme to solve the underlying thermo-mechanical problem is developed. In the present implementation, a displacement discontinuity (crack) is embedded perpendicular to the first principal direction in a linear triangle element upon violation of the Rankine criterion. In the thermo-mechanical problem, the heating due to mechanical dissipation is neglected as insignificant in comparison to the external heat flux. This leads to an uncoupled thermo-mechanical problem where the only input from the thermal part to the mechanical part is thermal strains. This problem is solved with explicit time marching using the mass scaling to speed up the solution. Finally, the fluid trapped into the micro-pores is modelled as a material that can bear only volumetric compressive stresses. A thermal spallation problem of a rock sample under axisymmetry is simulated as a numerical example.

In memory of Professor Emeritus Tapio Salmi

Introduction

Accessing geothermal energy in most parts of the globe is hampered by the high drilling costs incurred from using traditional drilling technologies based solely on the mechanical breakage of rock. For this reason, alternative drilling methods based on improved concepts and/or using some non-mechanical agents to enhance/replace the mechanical breakage are being searched presently. One such method is the thermal jet drilling (see [1]) based on the thermal spallation phenomenon illustrated in Figure 1.

Accordingly, when the surface of granite rock is heated rapidly (Figure 1a), the ensuing sharp temperature gradient induces a lateral compressive stress state into a layer adjacent to the rock surface (Figure 1b). Consequently, the favourably oriented inherent microcracks in rock grow (by the wing crack mechanism) parallel to the surface (Figure 1b) and, when the crack reaches the critical strength, a heated fragment buckles and is

ejected out as a spall (Figure 1c). The spallation is facilitated by mismatching elastic and thermal properties of the constituent rock minerals, i.e. discontinuities of the elastic and thermal properties at the mineral boundaries create stress concentrations that drive thermal cracking. According to the experiments by Kant and von Rohr [2], the minimal required temperature for spallation to occur in granite is about 500–600 °C.
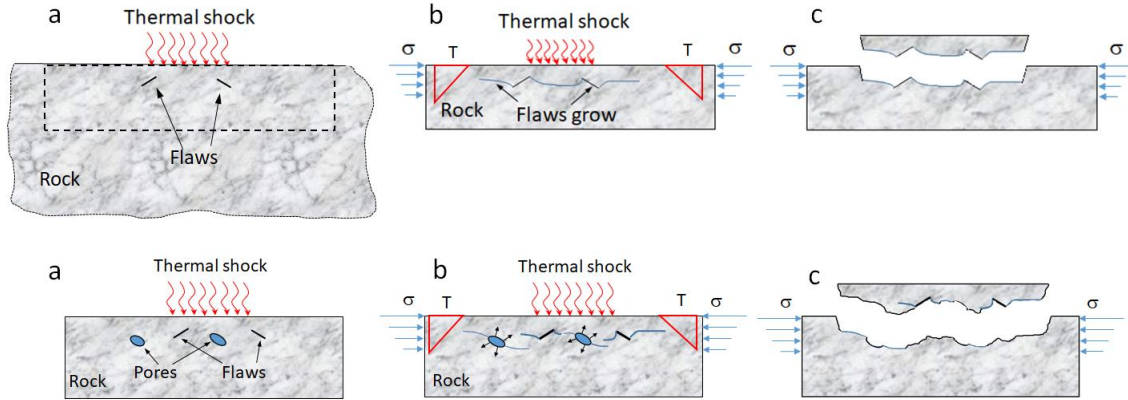

Figure 1. Principle of thermal spallation (upper row) and pore-fluid enhanced thermal spallation (lower row): In both cases, the stages are a) the heating of the rock surface, b) the build-up of the lateral stress field and the consequent crack propagation, and c) the resulting ejection of the chips called spalling.

Thermal spallation, or weakening rock by a heat shock in general, can be used in mining and excavation to assist/replace the traditional mechanical breakage, as mentioned above. For this reason, it has been the topic of several numerical studies, see [3–5] for example. In the paper by Walsh and Lomov [3], the authors proposed a modified version of the spallation model, illustrated in the lower row in Figure 1, where the heated fluid trapped in the micropores in granite enhances the spallation. Despite the low porosity (usually less than 1.5 %) of granite rocks, the fluid heated in the micropores served to increase the damage in their numerical simulations. In the present paper, the effect of pore-fluid on the spallation in granite is numerically studied.

For this end, a finite element based numerical method developed by Pressacco and Saksala [4] and Saksala [5] is further extended to account for the pore-fluid pressure. In this approach, the rock fracture is modelled by the embedded discontinuity finite elements [6]. In comparison to the external heat shock, the mechanical heating effects are insignificant. Therefore, the governing thermo-mechanical problem becomes uncoupled. Moreover, the material properties are assumed to be temperature independent in this preliminary study. A numerical example of heterogeneous granitic rock under a high intensity heat flux is solved with and without fluid-filled micro-pores under axisymmetric conditions in order to demonstrate the method.

Numerical model

A brief description of the modelling approach is given here. First, the finite element discretized equations of the thermal and mechanical parts of the problem are given. Then, the rock fracture model based on the embedded discontinuity finite elements is sketched. Finally, the time integration scheme of the uncoupled thermo-mechanical problem is outlined.

Finite element discretized heat equation and equation of motion

Modelling of the thermal spallation illustrated in Figure 1 requires solving the underlying thermo-mechanical problem. The thermal part is governed by the time-dependent heat equation, which can be written in the finite element discretized form as [7]

$$\mathbf{C}\dot{\boldsymbol{\theta}} + \mathbf{K}_\theta \boldsymbol{\theta} = \mathbf{f}_\theta + \mathbf{f}_Q \tag{1}$$

where $\mathbf{C}$, $\mathbf{K}_\theta$, $\mathbf{f}_\theta$ and $\mathbf{f}_Q$ are the capacitance matrix, the conductivity matrix, the external force, and the mechanical heating term, respectively, defined by

$$\mathbf{C} = \mathbf{A}_{k=1}^{N_e} \int_{V_e} \rho c \mathbf{N}_\theta^T \mathbf{N}_\theta dV, \quad \mathbf{K}_\theta = \mathbf{A}_{k=1}^{N_e} \int_{V_e} k \mathbf{B}_\theta^T \mathbf{B}_\theta dV$$

$$\mathbf{f}_\theta = -\mathbf{A}_{k=1}^{N_e} \int_{A_e} q_n \mathbf{N}_\theta^T dA, \quad \mathbf{f}_Q = \mathbf{A}_{k=1}^{N_e} \int_{V_e} Q \mathbf{N}_\theta^T dV \tag{2}$$

where ρ is the density, c is the specific heat capacity, θ is the temperature, $\mathbf{N}_\theta$ is the temperature interpolation matrix, k is the conductivity, q_n is the normal component of the heat flux, and $\mathbf{B}_\theta$ is the gradient of $\mathbf{N}_\theta$, and $\mathbf{A}$ is the standard finite element assembly operator . Generally, the specific heat capacity and conductivity depend on temperature, but this dependency is neglected in this study. Moreover, the convection at the boundaries of the rock specimen is also ignored as insignificant due to the short heating times. Finally, the term Q in (2) expresses the mechanical heat production through dissipation and strain rate. This term is ignored as insignificant in comparison to the external flux, hence $\mathbf{f}_Q \equiv \mathbf{0}$ from now on. This assumption makes the thermo-mechanical problem uncoupled facilitating its solution significantly [7].

The mechanical part of the problem, in the present explicit dynamics approach, is governed by the discretized equation of motion:

$$\mathbf{M}\ddot{\mathbf{u}} + \mathbf{f}_{int} = \mathbf{f}_{ext}$$

$$\mathbf{M} = \mathbf{A}_{k=1}^{N_e} \int_{V_e} \rho \mathbf{N}^T \mathbf{N} dV \tag{3}$$

$$\mathbf{f}_{int} = \mathbf{A}_{k=1}^{N_e} \int_{V_e} \mathbf{B}_u^T \boldsymbol{\sigma} dV$$

where $\mathbf{M}$ is the mass matrix, $\mathbf{N}$ is the displacement interpolation matrix, $\mathbf{u}$ is the displacement vector, $\boldsymbol{\sigma}$ is the stress matrix, $\mathbf{f}_{ext}$, $\mathbf{f}_{int}$ are the external and internal force vectors, respectively, $\mathbf{B}_u$ is the kinematic operator matrix.

Embedded discontinuity finite element model for rock fracture

The behavior of the rock is assumed linear elastic until the tensile strength is reached. After reaching the tensile strength, the fracture of rock is modelled with the embedded discontinuity concept, which is an element-based enrichment technique. Accordingly, upon reaching an elastic limit of a finite element, a discontinuity line (surface in 3D) is embedded inside the element. In the present version, the Rankine criterion is used to indicate cracking and the discontinuity is oriented orthogonal to the first principal direction. This failure criterion is chosen since the mode I fracture is the most common

fracture type in rocks irrespective of the loading conditions. A brief summary of the model originally presented by Saksala et al. [6] is given here.

When a displacement discontinuity (crack) is embedded in a CST (constant strain triangle) element, the displacement, $\mathbf{u}$, and strain, $\boldsymbol{\varepsilon}$, fields can be decomposed as

$$\mathbf{u} = N_i \mathbf{u}_i^e + (H_{\Gamma_d} - \varphi)\boldsymbol{\alpha}_d$$

$$\boldsymbol{\varepsilon} = \nabla N_i \otimes \mathbf{u}_i^e - \nabla\varphi \otimes \boldsymbol{\alpha}_d \qquad (4)$$

$$\nabla\varphi = \arg\left(\max_{k=1,2} \frac{\left|\Sigma_{i=1}^k \nabla N_i \cdot \mathbf{n}\right|}{\left\|\Sigma_{i=1}^k \nabla N_i\right\|}\right)$$

where $\boldsymbol{\alpha}_d$ is the displacement jump vector, N_i and $\mathbf{u}_i^e$ are the standard interpolation function and displacement vector at node i (summation applies on repeated i), and H_{Γ_d} is the Heaviside function at discontinuity Γ_d with normal $\mathbf{n}$. Finally, φ is a function that restricts the effect of the displacement jump within the corresponding finite element so that the essential boundary conditions remain unaffected. It should also be mentioned that the gradient of the displacement jump is assumed zero here, i.e. constant mode I and II discontinuity is adopted. Equation (4) specifies also how function φ is selected from among the nodal interpolants.

A bi-surface, plasticity inspired model was developed in Saksala et al. [6] for solving the displacement jump vector and the traction updates, as well as to control the softening behavior at the discontinuity. The components of this model are

$$\phi_t(\mathbf{t}_{\Gamma_d}, \kappa, \dot{\kappa}) = \mathbf{n} \cdot \mathbf{t}_{\Gamma_d} - (\sigma_t + q(\kappa, \dot{\kappa}))$$

$$\phi_s(\mathbf{t}_{\Gamma_d}, \kappa, \dot{\kappa}) = |\mathbf{m} \cdot \mathbf{t}_{\Gamma_d}| - (\sigma_s + \tfrac{\sigma_s}{\sigma_t} q(\kappa, \dot{\kappa}))$$

$$\dot{\boldsymbol{\alpha}}_d = \dot{\boldsymbol{\alpha}}_I + \dot{\boldsymbol{\alpha}}_{II} = \dot{\lambda}_t \frac{\partial\phi_t}{\partial\mathbf{t}_{\Gamma_d}} + \dot{\lambda}_s \frac{\partial\phi_s}{\partial\mathbf{t}_{\Gamma_d}} \qquad (5)$$

$$\dot{\mathbf{t}}_{\Gamma_d} = -\mathbf{E} : (\nabla\varphi \otimes \dot{\boldsymbol{\alpha}}_d) \cdot \mathbf{n}, \quad \dot{\kappa} = -\dot{\lambda}_t \frac{\partial\phi_t}{\partial q} - \dot{\lambda}_s \frac{\partial\phi_s}{\partial q}$$

$$q = h\kappa + s\dot{\kappa}, \quad h = -g\sigma_t \exp(-g\kappa)$$

$$\dot{\lambda}_i \geq 0, \quad \phi_i \leq 0, \quad \dot{\lambda}_i\phi_i = 0, \quad i = t,s$$

where ϕ_t and ϕ_s are the tension (mode I) and shear (mode II) loading functions, respectively, $\kappa, \dot{\kappa}$ are the internal variable and its rate, $\mathbf{m}$ is the crack tangent vector, σ_t and σ_s are elastic limits in tension and shear, respectively, $\boldsymbol{\alpha}_I$, $\boldsymbol{\alpha}_{II}$ are the mode I and II crack opening vectors, $\mathbf{E}$ is the elasticity tensor, $\dot{\lambda}_t$, $\dot{\lambda}_s$ are the mode I and II opening increments, respectively, h is the softening modulus, and s is the constant viscosity modulus. The softening slope parameter g is defined by the mode I fracture energy G_{Ic} by $g = \sigma_t/G_{Ic}$. Viscosity is included here, in the consistency format by Wang [8], to stabilize the computations, not to account for strain-rate effects, which are insignificant in the present type of problems.

The problem defined by model (5), i.e. the traction and internal variables update, can be solved with the standard algorithms of multi-surface plasticity [8]. After this, a new stress is calculated by

$$\boldsymbol{\sigma} = \mathbf{E} : (\boldsymbol{\varepsilon}_{\text{tot}} - \nabla\varphi \otimes \boldsymbol{\alpha}_d - \boldsymbol{\varepsilon}_\theta), \quad \boldsymbol{\varepsilon}_\theta = \alpha\Delta\theta\mathbf{I} \tag{6}$$

where $\boldsymbol{\varepsilon}_{\text{tot}}$ and $\boldsymbol{\varepsilon}_\theta$ are the total and thermal strain tensor, respectively, α is the thermal expansion coefficient, $\Delta\theta$ is the temperature difference, and $\mathbf{I}$ is the identity tensor.

Finally, the method for modelling the pore-fluid is explained. A very rough approximation is taken here assuming that the fluid in micro-pores is a material that can withstand only compressive volumetric stress, i.e. pressure. Thereby, for the elements designated as modelling the pore-fluid the stress-strain relation is

$$\boldsymbol{\sigma} = K_{\text{bulk}}(\varepsilon_{\text{vol}} - \alpha\Delta\theta)\mathbf{I} \tag{7}$$

where K_{bulk} is the elastic bulk modulus of the fluid, and ε_{vol} is the volumetric strain. Thus, in this scheme fluid flow of any kind is neglected and possible phase changes are ignored. The purpose of this simple model is to test if the thermal expansion of the pore-fluid enhances the spallation.

Explicit scheme for solving the uncoupled thermo-mechanical problem

The uncoupled thermo-mechanical problem governing the thermal spallation is solved with explicit time marching. The forward Euler method is employed here leading to following equation for the new temperature $\boldsymbol{\theta}_{n+1}$:

$$\mathbf{C}_n\boldsymbol{\theta}_{n+1} = (\mathbf{C}_n - \Delta t\mathbf{K}_{\theta,n})\boldsymbol{\theta}_n + \Delta t\mathbf{f}_{\theta,n} \tag{8}$$

The mechanical update is performed as follows:

$$\begin{aligned}
\mathbf{M}\ddot{\mathbf{u}}_t + \mathbf{f}_{\text{int},t} &= \mathbf{f}_{\text{ext},t} \rightarrow \ddot{\mathbf{u}}_t \\
\dot{\mathbf{u}}_{n+1} &= \dot{\mathbf{u}}_n + \Delta t\ddot{\mathbf{u}}_t \\
\mathbf{u}_{n+1} &= \mathbf{u}_n + \Delta t\dot{\mathbf{u}}_{n+1}
\end{aligned} \tag{9}$$

Now, the solution procedure is as follows. First, the temperature is solved by Equation (8) since the temperature is needed to calculate the stress by Equation (6). Then, if an element has no crack and it is not a pore-fluid element, the Rankine criterion is checked and if violated, a crack (discontinuity) is embedded to that element and the model (5) is solved consequently for the new crack and for an old crack if the loading functions in (5) are violated. Note that only one crack with a fixed orientation is allowed per element. For a pore-fluid element, the stress is calculated by Equation (7). Finally, the mechanical response is advanced by solving (9).

Numerical simulations

A problem thermal spallation of rock is simulated here in order to test whether the fluid in micro-pores enhance the spallation if granitic rock. Numerical rock is assumed to be heterogeneous with three different minerals (Quartz, Feldspar, and Biotite). This is the appropriate approach as no real rock can be considered homogeneous at the scale (a disc with radius of 15 mm and thickness of 5 mm) considered here. The heterogeneity is described as follows. First, the element numbers are assigned with integers from 1 to 3 corresponding to the percentage of the minerals in rock. For example, if the real rock has 33 % of Quartz, then 33 % percent of the elements in the mesh are designated as

Quartz. Then, the sets representing different minerals are randomly mapped into the mesh resulting in a mesoscopic description of heterogeneity. The material and model properties for minerals and the pore-fluid (water) are in Table 1. The homogenized values for the minerals, calculated by the rule of mixtures ($x_{mix} = \sum f_i x_i$, f_i being the volume fraction of phase i), are also given in Table 1.

Table 1: Material and model parameter for typical minerals found in granitic rocks

Parameter	Quartz	Feldspar	Biotite	Homog	Water	Equation
%	33	50	12/17	100	5/0	
ρ [kg/m^3]	2650	2620	3050	2703	1000	(2), (3)
E [GPa]	80	60	20	59.8	2.15*	(5), (6)
ν	0.17	0.29	0.20	0.235	-	(5), (6)
σ_t [MPa]	10	8	7	8.49	0	(5)
σ_s [MPa]	50	50	50	50	0	(5)
G_{Ic} [J/m^2]	40	40	28	38	0	(5)
α [1/K]	1.60E–5	0.75E–5	1.21E–5	1.12E–5	2.07E–4	(6), (7)
k [W/mK]	4.94	2.34	3.14	3.33	0.6	(2)
c [J/kgK]	731	730	770	737	4185	(2)

*Bulk modulus

The explicit schemes for solving the thermal and mechanical problems (8) and (9) have vastly differing time scales and hence the critical time steps. For this reason, mass scaling is used for the mechanical problem to speed up the solution in time. Fortunately, the present problem turned out to be especially suitable for extreme mass scaling: numerical tests revealed that the response remained virtually identical even when the density for the mechanical part of the problem was 10000-fold resulting in a critical time step of 100 times larger than that with the original density.

The boundary conditions and the numerical rock are shown in Figure 2. In order to test the effect of the pore-fluid, a percentage of the elements in the mesh representing Biotite is assigned to pores as indicated in Table 1.
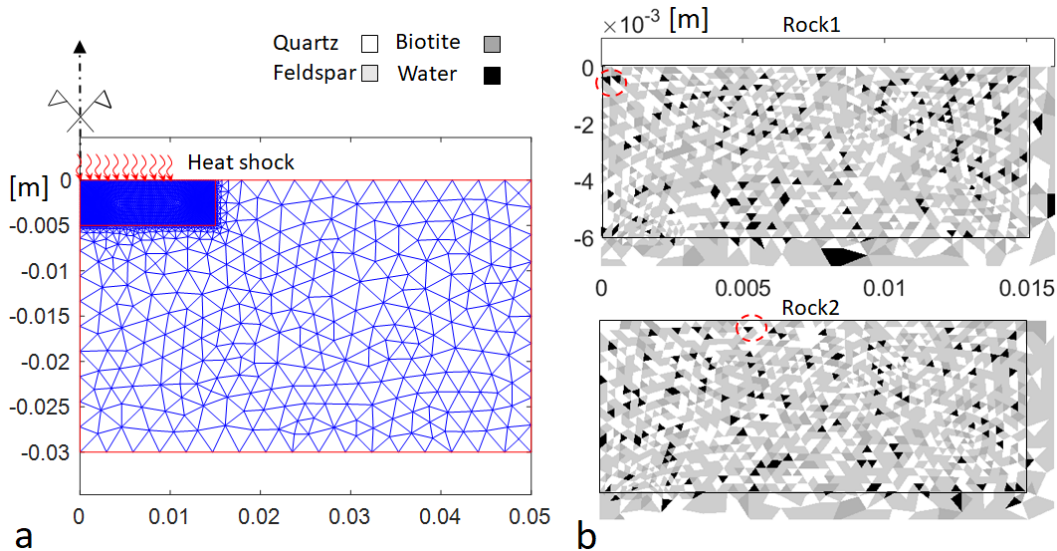

Figure 2. The CST mesh with 2963 elements and boundary conditions a), and the numerical rock samples b) (the critical elements representing water are indicated by a red circle).

The average element size in the area under the heat shock is about 0.3 mm leading to a critical time step of order 1E−8 s. Therefore, the mass-scaled time step is of order 1E−6 s requiring quite short practical analysis times. Here, a heating time of 0.1 s is set, and the intensity of the thermal shock is q_n = 3E6 J/m^2. The heat shock is spatially and temporally constant and the radius of the heated part of the surface is 10 mm. The initial condition for the thermal part is the room temperature, i.e. 20 °C, which means that shallow conditions (close to surface) without any confinement or overburden pressure are assumed here. As mentioned above, convection at the rock boundaries is ignored – an assumption justified by the short duration of the heating process. First, a simulation with the homogenized material properties is carried out in order to illustrate the general features of the problem. The results are shown in Figure 3.

Due to the short heating time, the temperature rises only in a thin (~ 1 mm) layer of the rock sample (see Figure 3c) while the final temperature at the flux nodes is about 400 °C (Figure 3d). The resulting radial and axial stress distributions plotted in Figure 3a and b, respectively, show that a 1 mm thick surface layer of rock is in compressive stress state in the radial direction. Below this layer, both stress components are tensile in nature. These features of the thermal stresses are accordingly reflected in the induced crack orientation distribution shown in Figure 3f: The cracks at the compressive zone close to the rock surface are parallel to the surface while more vertically oriented cracks are attested in the tensile stress zone. The corresponding crack opening magnitudes shown in Figure 3e are so mild that no spallation is expected here. Indeed, the maximum opening was 5.6E–4 mm in the element in the right upper corner in Figure 3e. This value corresponds to q = –4.5 MPa (see Equation (5)) so that only about 50 % of the tensile strength (8.49 MPa) is exhausted.

In passing, an anomaly in the stresses in Figure 3b is observed. Namely, the vertical stress component displays a checkerboard pattern (i.e. an alternation of the stress from compression to tension in adjacent elements) in the layer where the radial stress in compressive. This is quite common behavior for the CST element with certain kinds of structured meshes in analyses involving incompressible material. However, the material behavior here neither is incompressible nor is the mesh structured. Still, this anomaly is probably due to the low order kinematics of the CST element. Anyways, further elaboration is beyond the scope of this paper.

Next, the same problem is simulated with heterogeneous rock using the numerical rock sample Rock1. The results are shown in Figure 4.

Due to the heterogeneous rock, the crack orientations are now more random than with the homogeneous rock, as can be seen in Figure 4a. Moreover, the final surface temperatures vary from 360 to some 490 °C (Figure 4b), which has led to a much more severe damage in terms of crack opening magnitudes shown in Figure 4c. The crack opening at one of the elements close to rock surface at the symmetry axis exceeds 1 mm, as can be observed in the Figure 4c. Within the present small strain continuum modelling context, this can be interpreted as a numerical representation of spallation, albeit extremely local one. When the pore-fluid is included, the spallation is predicted to start at t = 0.069 s as the two elements representing fluid-filled pores close to the origin of the axes (see Rock1 in Figure 2b) cause the surrounding elements to fail violently (Figure 4d). It should be noted that these elements do not have cracks. Moreover, the thermal expansion coefficient of the pore-fluid (water) is about 20 times larger than that of the surrounding rock mineral elements (see Table 1).

Finally, the simulation is repeated with the numerical rock sample Rock2. The results are presented in Figure 5 only for the crack opening magnitudes with and without the pore-fluid. It should be kept in mind that the underlying mesh is the same in all three simulated cases, only the mineral phases, i.e., the random clusters representing different minerals, are different in Rock1 and Rock2.
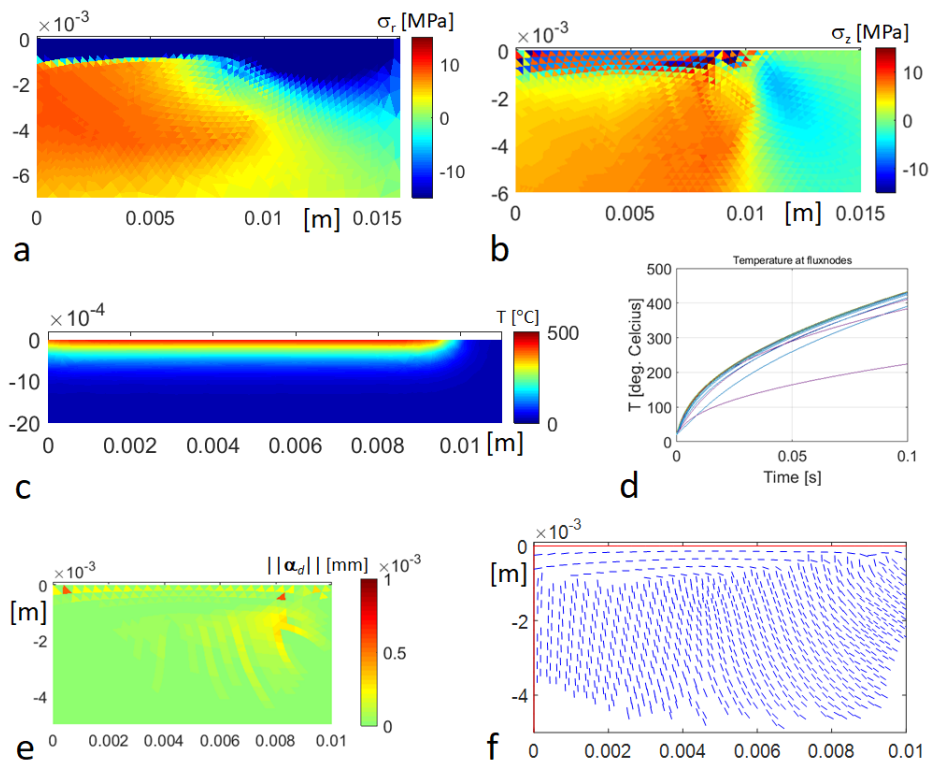
Figure 3. Simulation results with homogenized material: Radial (a) and vertical (b) stress components (tensile stresses are positive), temperature distribution (c), temperature at the flux nodes as a function of time (d), crack openings (e), and crack orientations (f) at the end of simulation.
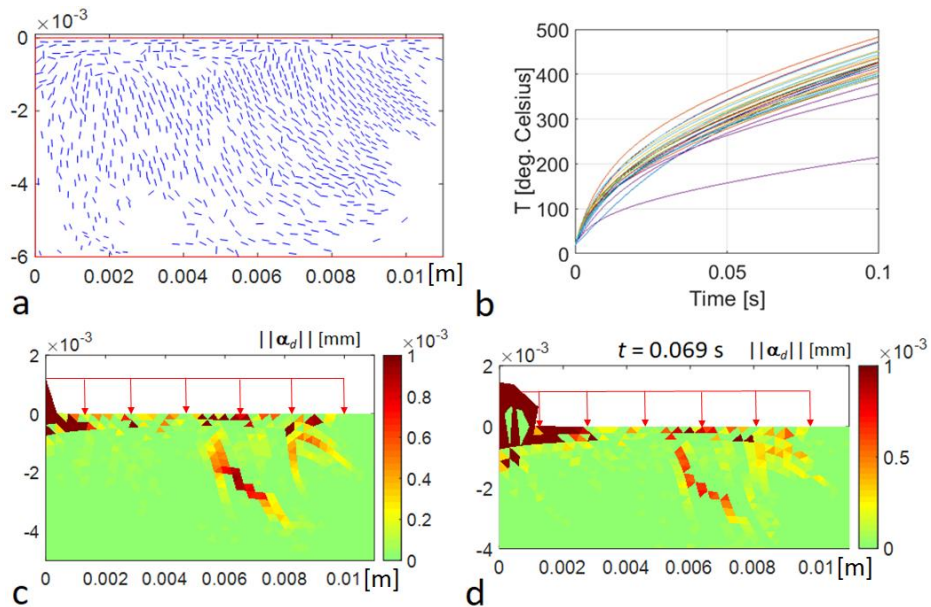

Figure 4. Simulation results with numerical rock Rock1: Crack orientations (a), temperature at the flux nodes as a function of time (b), crack openings without pore-fluid at the end of simulation (c), and crack openings with pore-fluid at $t = 0.069$ s (d).
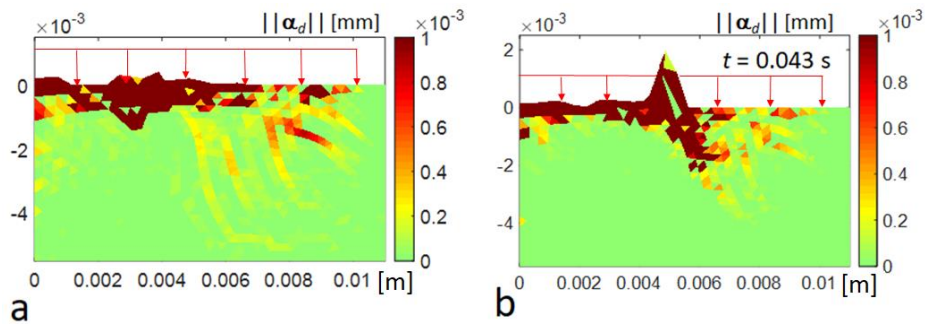
Figure 5. Simulation results with numerical rock Rock2: Crack openings without pore-fluid at the end of simulation (a), and crack openings with pore-fluid at $t = 0.043$ s (b).

With the numerical rock sample Rock2, the spallation predicted at the end of the simulation is substantially wider than with Rock1, as can be observed in Figure 5a. Indeed, a spall with thickness varying from 0.3 to 1 mm and width of 7 mm is predicted without the pore-fluid. With the pore-fluid, again, a violent local spallation is predicted to take place at $t = 0.043$ s in addition to the ejection of the surface elements (the critical element where this behavior is originated is circled in Figure 2b).

Conclusions

A numerical method to model pore-fluid enhanced thermal spallation of rock based on embedded discontinuity finite elements was presented. The mechanical heating effects were ignored as insignificant compared to the external heat shock. Thereby, the finite element discretized uncoupled thermo-mechanical problem was solved with explicit time marching using the mass-scaling for the mechanical part to increase the critical time step. The pore-fluid was modelled as a material that can withstand only negative volumetric stresses. In the numerical simulations, the effect of pore-fluid on the spallation was tested. The simulations confirm the hypothesis that the presence of the pore-fluid enhances the spallation of granitic rock.

As no real rock can be plausibly considered homogeneous at the scale of consideration of present simulations, heterogeneity of rock was described as random clusters of finite elements representing the constituent minerals. The two considered random rock samples resulted, with the present setup, in two different, representative kinds of behaviour; minimal to no spallation, and critical spallation. These simulations thus demonstrate that mesostructural details may have, at least locally, a substantial effect on the resulting failure behaviour of rock under intensive thermal loading.

Acknowledgements

References

[1]   E. Rossi, M.A. Kant, C. Madonna, M.O. Saar, P.R. von Rohr. The Effects of High Heating Rate and High Temperature on the Rock Strength: Feasibility Study of a Thermally Assisted Drilling Method. *Rock Mechanics and Rock Engineering*, 51: 2957—2964, 2018. https://doi.org/10.1007/s00603-018-1507-0

[2]   M.A. Kant, P.R. von Rohr. Minimal required boundary conditions for the thermal spallation process of granitic rocks. *International Journal of Rock Mechanics & Mining Sciences*, 84:177–186, 2016. https://doi.org/10.1016/j.ijrmms.2015.12.009

[3]   S.D.C. Walsh, I.N. Lomov. Micromechanical modeling of thermal spallation in granitic rock. *International Journal of Heat and Mass Transfer*, 65:366–373, 2013. https://doi.org/10.1016/j.ijheatmasstransfer.2013.05.043

[4]   Pressacco, M., Saksala, T., Numerical modelling of fracture process in thermal shock weakened rock. In: Litvinenko v. (Ed.) Proceedings of the 2018 European Rock Mechanics Symposium (EUROCK2018: Geomechanics and Geodynamics of Rock Masses), Saint Petersburg, Russia, 22–26 May, 2018. Vol 1, pp. 883–888.

[5]   T. Saksala. Numerical modelling of thermal spallation of rock. Proceedings of XII Argentine Congress on Computational Mechanics (MECOM2018), 6–9 November 2018, Tucuman, Argentina.

[6]   T. Saksala, D. Brancherie, I. Harari, A. Ibrahimbegovic. Combined continuum damage-embedded discontinuity model for explicit dynamic fracture analyses of quasi-brittle materials. *International Journal for Numerical Methods in Engineering*, 101:230–250, 2015. https://doi.org/10.1002/nme.4814

[7]   N.S. Ottosen, M. Ristinmaa. *The Mechanics of Constitutive Modeling*. Elsevier: Amsterdam, 2005.

[8]   W.M. Wang, L.J. Sluys, R. De Borst. Viscoplasticity for instabilities due to strain softening and strain-rate softening. *International Journal for Numerical Methods in Engineering*, 40:3839-3864, 1997. https://doi.org/10.1002/(SICI)1097-0207(19971030)40:20<3839::AID-NME245>3.0.CO;2-6

Timo Saksala
Laboratory of Civil Engineering, Tampere University
P.O. Box 600, FI-33101 Tampere
timo.saksala@tuni.fi